Ligand Binding to Heme Proteins. VI. Interconversion of Taxonomic Substates in Carbonmonoxymyoglobin

J. Bruce Johnson, Don C. Lamb, Hans Frauenfelder, Joachim D. Müller, Ben McMahon, G. Ulrich Nienhaus, Robert D. Young

Department of Physics, University of Illinois at Urbana-Champaign, Urbana, Illinois 61801-3080 USA

ABSTRACT The kinetic properties of the three taxonomic A substates of sperm whale carbonmonoxy myoglobin in 75% glycerol/buffer are studied by flash photolysis with monitoring in the infrared stretch bands of bound CO at $\nu(A_0) \approx 1967$ cm^{-1}, $\nu(A_1) \approx 1947$ cm^{-1}, and $\nu(A_3) \approx 1929$ cm^{-1} between 60 and 300 K. Below 160 K the photodissociated CO rebinds from the heme pocket, no interconversion among the A substates is observed, and rebinding in each A substate is nonexponential in time and described by a different temperature-independent distribution of enthalpy barriers with a different preexponential. Measurements in the electronic bands, e.g., the Soret, contain contributions of all three A substates and can, therefore, be only approximately modeled with a single enthalpy distribution and a single preexponential. The bond formation step at the heme is fastest for the A_0 substate, intermediate for the A_1 substate, and slowest for A_3. Rebinding between 200 and 300 K displays several processes, including geminate rebinding, rebinding after ligand escape to the solvent, and interconversion among the A substates. Different kinetics are measured in each of the A bands for times shorter than the characteristic time of fluctuations among the A substates. At longer times, fluctuational averaging yields the same kinetics in all three A substates. The interconversion rates between A_1 and A_3 are determined from the time when the scaled kinetic traces of the two substates merge. Fluctuations between A_1 and A_3 are much faster than those between A_0 and either A_1 or A_3, so A_1 and A_3 appear as one kinetic species in the exchange with A_0. The maximum-entropy method is used to extract the distribution of rate coefficients for the interconversion process $A_0 \leftrightarrow A_1 + A_3$ from the flash photolysis data. The temperature dependencies of the A substate interconversion processes are fitted with a non-Arrhenius expression similar to that used to describe relaxation processes in glasses. At 300 K the interconversion time for $A_0 \leftrightarrow A_1 + A_3$ is 10 μs, and extrapolation yields $\sim$1 ns for $A_1 \leftrightarrow A_3$. The pronounced kinetic differences imply different structural rearrangements. Crystallographic data support this conclusion: They show that formation of the A_0 substate involves a major change of the protein structure; the distal histidine rotates about the C_α–C_β bond, and its imidazole sidechain swings out of the heme pocket into the solvent, whereas it remains in the heme pocket in the $A_1 \leftrightarrow A_3$ interconversion. The fast $A_1 \leftrightarrow A_3$ exchange is inconsistent with structural models that involve differences in the protonation between A_1 and A_3.

PROTEIN SUBSTATES AND FUNCTION

Protein substates

Many proteins possess at least two states. Myoglobin, for instance, exists in the ligand-bound form (MbO_2 or MbCO) or in the deoxy form (Mb). If each state were unique and rigid, adaptation would be difficult. Within each state, however, a protein can assume a large number of conformational substates (CSs) that endow the protein with flexibility (Austin et al., 1975; Frauenfelder et al., 1978, 1988, 1991; Elber and Karplus, 1987). Proteins in different CSs perform the same function but usually with different rates. At physiological temperatures, proteins fluctuate among the thermally accessible CSs. The environment controls protein reactions by modifying the energies, entropies, and volumes of the CSs, thus changing the relative populations (Ansari et al., 1987; Morikis et al., 1989; Frauenfelder et al., 1990; Hong et al., 1990; Zhu et al., 1992).

The CSs in sperm whale MbCO are arranged in a hierarchy that consists of a number of tiers (Ansari et al., 1985, 1987; Frauenfelder et al., 1991; Steinbach et al., 1991). In tier 0 the barriers between the valleys in the energy hypersurface are largest, and three taxonomic substates, denoted A_0, A_1, and A_3, can be distinguished. These A substates are characterized by the infrared absorption bands of the bound CO, $\nu(A_0) \approx 1967$ cm^{-1}, $\nu(A_1) \approx 1947$ cm^{-1}, and $\nu(A_3) \approx 1933$ cm^{-1}. Equilibrium populations of the A substates depend on external conditions such as temperature, pH, solvent composition, and pressure (Ansari et al., 1987; Hong et al., 1990; Iben et al., 1989; Frauenfelder et al., 1990; Morikis et al., 1989; Zhu et al., 1992; Mourant et al., 1993). Below 160 K, conformational transitions between the A substates do not occur, and rebinding of CO after photodissociation to each individual A substate is nonexponential in time. Therefore, the population within each A

Received for publication 10 October 1995 and in final form 17 June 1996.

Address reprint requests to Dr. Gerd Ulrich Nienhaus, Abt. Biophysik, Universität Ulm, Albert-Einstein-Allee 11, 89081 Ulm, Germany. Tel.: 49-731-502-3050; Fax: 49-731-502-3059.; E-mail: uli@uiuc.edu.

H. Frauenfelder's current address is CNLS, Los Alamos National Laboratory, Los Alamos, NM 87545.

J. B. Johnson's current address is Department of Physics, Arkansas State University, State University, AR 72467.

D. C. Lamb's current address is Physik-Department E17, Technische Universität München, 85748 Garching, Germany.

R. D. Young's current address is Department of Physics, Illinois State University, Normal, IL 61761.

0006-3495/96/09/1563/11 $2.00

substate is kinetically inhomogeneous; each substate of tier 0 in MbCO comprises a large number of substates of tier 1.

Although MbCO is one of the best-studied proteins, the protein–ligand interactions that give rise to the different *A* substates are still under intensive study (see, for instance, Springer et al., 1994). Recent Fourier-transform IR studies of a large number of distal pocket mutants have elucidated how structural modifications in the distal pocket affect the IR bands of bound CO (Braunstein et al., 1993; Li et al., 1994). They showed that electrostatic interactions between the bound CO and the residues lining the heme pocket play an important role. Especially important is the interaction with the key distal residue His-E7. Further information comes from NMR (Park et al., 1991), resonance Raman experiments (Ray et al., 1994), and x-ray crystallography (Quillin et al., 1992; Yang and Phillips, 1995). Whereas the nature of the A_0 substate is clarified, disagreement still exists over the assignment of A_1 and A_3 (Oldfield et al., 1991; Ray et al., 1994; Li et al., 1994; Jewsbury and Kitagawa, 1994).

Taxonomic substates exist in a number of carbonmonoxy heme proteins. In MbCO the existence of *A* substates is clearly indicated by the appearance of different CO stretch bands (Makinen et al., 1979; Alben et al., 1982; Shimada and Caughey, 1982). Many other heme proteins, for instance, cytochrome oxidase (Alben et al., 1981), cytochrome P450 (Tsubaki et al., 1986; Porter and Coon, 1991), horseradish peroxidase (Doster et al., 1987; Uno et al., 1987), and hemoglobin (Potter et al., 1990), all exhibit multiple CO stretch bands in the CO-ligated form and thus possess *A* substates. Taxonomic substates are also observed in other classes of protein, for example, retinal proteins and blue copper proteins (Nar et al., 1991; Ehrenstein et al., 1995). Theoretical ideas suggest that these substates are a general property of proteins (Honeycutt and Thirumalai, 1990). The observation of taxonomic substates in many proteins makes the investigation of their dynamic properties in MbCO relevant beyond the working of a single protein. The focus of this paper is on conformational transitions between the *A* substates.

Protein function and control

Using many different distal pocket mutants, Li et al. (1994) investigated correlations between the frequencies of the IR stretch bands of the bound CO in myoglobin and the overall dissociation and association rates. They showed that the dissociation rates at room temperature, measured for many different distal pocket mutants, correlate well with the wave number of the CO, reflecting an increase in bond strength between Fe and CO with decreasing ν_{CO}, as expected from the backbonding relation (see Discussion and Conclusions). The correlation between the association rates and ν_{CO} was much worse. This behavior is expected because the bound state does not necessarily bear information about how it was formed. Ligand binding is a complicated multistep process and, for example, displacement of water from the distal pocket and other steric effects may slow the binding without leaving an imprint on the interaction of the bound CO with distal pocket residues (Li et al., 1994). Infared kinetic experiments over wide temperature ranges enable us to separate kinetic processes that contribute to the overall rebinding rate coefficients.

The presence of multiple taxonomic substates with different ligand binding properties in myoglobin is a nice example of how the function of a protein can be controlled by the environment (Ansari et al., 1987; Frauenfelder et al., 1989). The environment can influence the relative populations of taxonomic substates, for example, by changing the pH. The overall association coefficient λ is given by (Frauenfelder et al., 1989)

$$\lambda = \sum c_i \lambda_i, \quad (1)$$

where c_i is the fractional population and λ_i is the rate coefficient of substate *i* in deoxy Mb. Because the different substates bind CO at different rates, the overall binding rate changes with the relative populations. Experimental evidence supporting this scenario has come from kinetic absorption and Raman studies of ligand association and dissociation rate coefficients in sperm whale Mb as a function of pH (Doster et al., 1982; Tian et al., 1993). Detailed understanding of such a control mechanism requires knowledge of the rate coefficients for interconversion among taxonomic substates.

In the bound state, conformational transitions among the *A* substates occur. We previously published MbCO rebinding kinetics monitored in the A_0 substate between 230 and 260 K that showed evidence for the interconversion process $A_0 \leftrightarrow A_1 + A_3$ in 75% glycerol/buffer (Young et al., 1991; Steinbach et al., 1992). Double-pulse flash photolysis experiments of the rebinding of MbCO confirmed these results (Tian et al., 1992). Here we report flash photolysis studies of the interconversion processes $A_1 \leftrightarrow A_3$ and $A_0 \leftrightarrow A_1 + A_3$ in sperm whale MbCO between 200 and 300 K. The results are compared with measurements made with pressure relaxation techniques (Iben et al., 1989; Frauenfelder et al., 1990; Scholl, 1991).

METHODS

Sample preparation

Samples for flash photolysis with monitoring in the visible were prepared as described previously (Steinbach et al., 1991). For flash photolysis in the IR, samples with a final protein concentration of 15 mM in a glycerol/buffer solvent (75%/25% v/v) were used. Samples at pH 5.7, in which a significant fraction of the population is in each of the three *A* substates, were prepared with 1.3 M potassium citrate buffer (p*H* 4.3). Samples at pH 9.1, prepared with potassium carbonate buffer (pH 11.0), were used to study the $A_1 \leftrightarrow A_3$ exchange because they show essentially only these two substates (Ansari et al., 1987; Morikis et al., 1989; Hong et al., 1990).

Spectroscopic methods

Flash photolysis experiments were conducted on two systems, one monitoring in the visible (Soret band at 440 nm) and one monitoring in the IR

CO stretch bands (~5 μm). The flash system with monitoring in the visible was described previously (Steinbach et al., 1991). In the IR flash photolysis system a 300-ns (full width at half maximum) pulse from a dye laser (model DL2100C; Phase-R, New Durham, NH), lasing broadband at 530 nm with 100 mJ of energy, photodissociated the sample. Rebinding was monitored with a lead-salt laser diode (Laser Photonics, Analytics Division, Bedford, MA). It was tunable from 1900 to 2000 cm^{-1} and focused on the sample, monochromator, and detector with calcium fluoride optics. The monochromator was used only for wavelength determination or rejection of unwanted modes because each mode of the IR laser diode is ~3 × 10^{-4} cm^{-1} wide. The signal from the photovoltaic InSb IR detector (Infrared Associates, Cranbury, NJ) was digitized with a logarithmic time-base digitizer from 1 μs to 1 ks. A closed-cycle helium refrigerator (Helix Technology Corp., CTI Cryogenics Division, Waltham, MA) cooled the laser diode and the sample.

Data analysis

The absorbance change in the sample that is due to the photolyzing laser flash is given by $\Delta A(t) = log(I(0^-)/I(t))$, where $I(0^-)$ is the intensity measured before photolysis and $I(t)$ is the intensity of light measured through the sample after photolysis. We divide $\Delta A(t)$ by the maximal absorbance change, ΔA_{max}, to obtain the normalized absorbance change, $N(t)$, which is the fraction of molecules in the dissociated state at time t after photolysis. It can be represented by a spectrum of exponential rate processes,

$$N(t) = \int d(\log \lambda) f(\lambda) e^{-\lambda t}. \quad (2)$$

The rate distribution function $f(\lambda)$ gives the probability density for absorbance changes with rate coefficient λ on a logarithmic scale. In the IR experiments described in this paper the absorbance changes arise not only from rebinding but also from a net flow of population from one A substate to another (vide infra).

We employ various numerical inversion techniques to extract $f(\lambda)$ from the $N(t)$ curves (Steinbach et al., 1992). Data analysis using the maximum-entropy method and Gaussian model fits led to essentially the same results. Here we calculate $f(\lambda)$ with the maximum-entropy method (MEM), a technique that can be used whenever the measured data represent a transform of the function of interest. Inevitably, experimental data are always incomplete and subject to noise. The MEM algorithm selects from the many solutions that fit the data equally well, namely, those with a normalized χ^2 of 1, a unique solution that is free of spurious correlations. We employ the MEM to extract rate distributions from individual kinetic traces by inversion of Eq. 2, and we also use a "global MEM," in which the algorithm was modified to study the interconversion between the A substates by simultaneously analyzing kinetics data of the three different A substates. In the global MEM the absorbance changes are modeled by a rebinding rate distribution $f_i(\lambda)$ for each A_i substate plus one exchange distribution $f_e(\lambda)$ that describes the transfer of population from A_0 to A_1 + A_3. With an appropriately modified definition of the entropy S, the method yields the most probable set of rate distributions, $f_i(\lambda)$ and $f_e(\lambda)$. For technical details, we refer the reader to the paper by Steinbach et al. (1992).

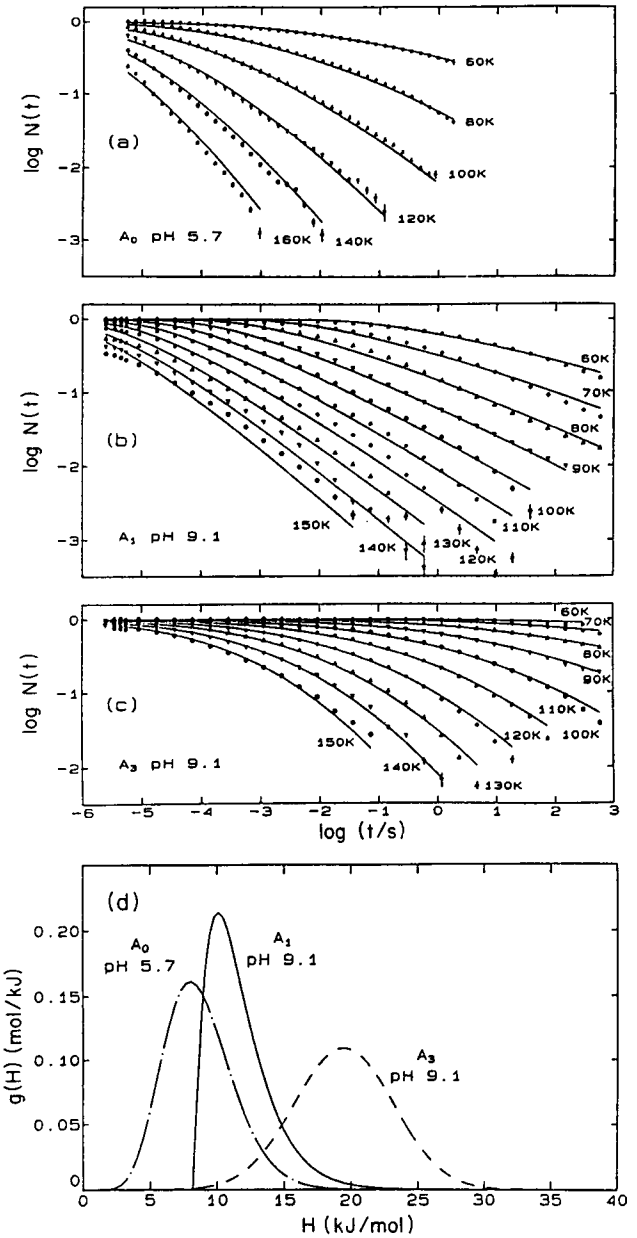

FIGURE 1 Ligand rebinding between 60 and 160 K. The fraction of myoglobin without a CO bound to the heme iron, $N(t)$, as a function of time after photolysis is shown for (*a*) A_0, (*b*) A_1, (*c*) A_3. (*d*) The distribution of activation enthalpy barriers $g(H_{BA})$ that generates the fits shown as solid curves in *a–c*. To fit $g(H_{BA})$, a gamma function was used for A_0 and A_1 and a Gaussian for A_3. Solvent: 75% glycerol/water (v/v).

RESULTS

Low-temperature rebinding

Below 160 K, ligands do not escape into the solvent but rebind geminately from the heme pocket. Moreover, there are no interconversions between taxonomic substates, and measurements of the transient absorbance changes in the CO stretch bands yield the rebinding to the individual A substates, as shown in Fig. 1, *a–c*. The kinetics of the different A substates differ considerably, with A_0 being fastest and A_3 being slowest. They are nonexponential, reflecting an inhomogeneous population of myoglobin molecules that possess different activation enthalpies H_{BA} and consequently rebind ligands with different rates. The fraction of molecules within each A substate that have not rebound a ligand at time t after photolysis, $N_i(t)$, is given by (Austin et al., 1975)

$$N_i(t) = \int dH_{BA} g_i(H_{BA}) e^{-k(H_{BA},T)t}, \quad (3)$$

where the inhomogeneous population within each taxonomic substate is characterized by a single, temperature-independent distribution of barriers, $g_i(H_{BA})$. Above ~50 K, the rate coefficient $k(H_{BA}, T) = A_{BA}(T/T_0)\exp(-H_{BA}/RT)$, where T_0 is a reference temperature taken to be 100 K.

The $g_i(H_{BA})$ distributions for rebinding to the three A substates are plotted in Fig. 1 *d*, and the parameters are listed in Table 1. For comparison we also give peak enthalpies as calculated from temperature-derivative spectroscopy measurements (Berendzen and Braunstein, 1990), using the preexponential values A_{BA} obtained from the data presented in this paper. We see good agreement of the H_{peak} parameter for temperature-derivative spectroscopy and IR flash photolysis for the three A substates. The solid curves in Fig. 1, *a–c* show rebinding curves calculated from the $g_i(H_{BA})$ distributions using Eq. 3. Whereas the A substate populations depend on pH, the $g_i(H_{BA})$ distributions are essentially pH independent (Mourant et al., 1993).

Flash photolysis studies with infrared monitoring above 200 K

Comparison of Soret and infrared kinetics

Experiments probing electronic bands in the visible measure the overall rebinding and do not distinguish among different taxonomic substates. Infrared monitoring, however, yields additional information about substate transitions.

Flash photolysis data above 200 K reflects a complex behavior. Undulations on the kinetic traces can be resolved into several peaks in the rate distribution function $f(\lambda)$ by the MEM. Fig. 2 shows the Soret rebinding kinetics between 200 and 300 K together with $f(\lambda)$ for 230 and 250 K. In Fig. 2 *b* various peaks, labeled 1–3 and S, stand out. This pattern is found in all Soret data between 200 and 250 K. At $T \geq 250$ K, separate peaks 1 and 2 are no longer observed (Fig. 2 *c*).

Fig. 3 shows the corresponding data for monitoring in the IR at the position of the A_1 band. In Fig. 3 *a* the experimental data are shown as points, whereas the solid curves are calculated with Eq. 2 from the rate distributions $f_1(\lambda)$, which are shown for 230 and 250 K as solid curves in Fig. 3, *b* and *c*. Differences between measured and calculated data are very small and cannot be visualized on any reasonable scale. Thus, we plotted the differences between measured and calculated transmittance data, $\Delta\mathcal{T}$, normalized to the statistical noise of the data (standard deviation $\sigma \approx 10^{-4}$ in transmittance), in the bottom parts of Fig. 3, *b* and *c*. The IR kinetics show the same general pattern of peaks as the Soret data, with consistent peak positions over the entire temperature range. However, the IR data reveal an additional peak, labeled E. At 230 K this peak is still ambiguous from the A_1 kinetics alone. We have labeled it here only because of the additional information from the A_0 kinetics, which we discuss below. At 250 K, however, Peak E is clearly visible and calls for an explanation.

To demonstrate the ability of the MEM to resolve the various peaks, we have included as dashed curves in Fig. 3, *b* and *c* results from MEM calculations that were aborted at

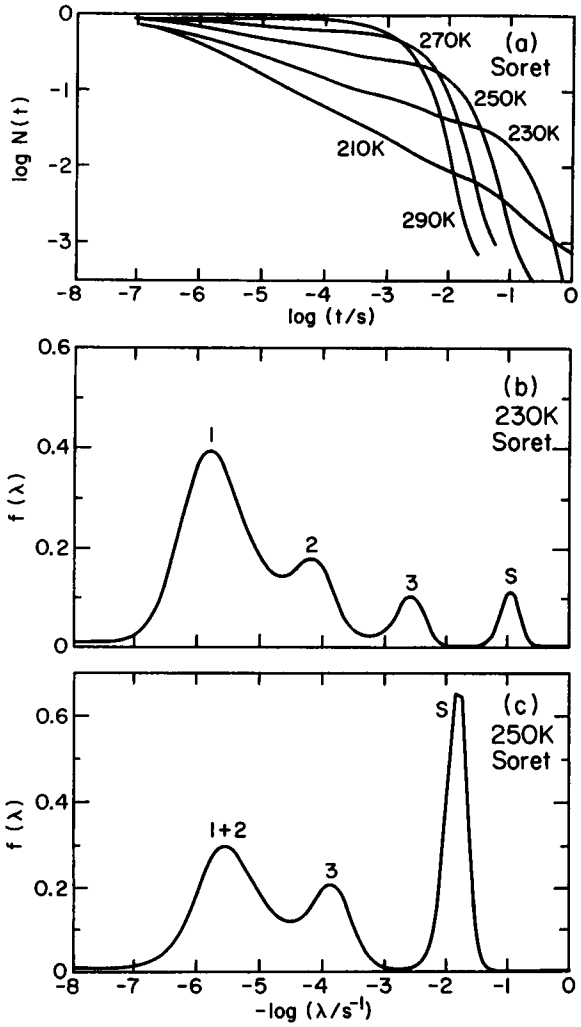

FIGURE 2 Rebinding kinetics and rate distributions of sperm whale MbCO measured in the Soret band. (*a*) Survival probability in the unbound state after photolysis, $N(t)$. Rate distribution functions $f(\lambda)$ at (*b*) 230 K and (*c*) 250 K, calculated using the MEM. Peaks 1–3 and S are discussed in the text. Solvent: 75% glycerol/water (v/v), pH 6.8.

TABLE 1 Parameters characterizing the geminate rebinding in MbCO at low temperature

Marker	$\log(A_{BA}/s^{-1})$	H_{peak} (kJ/mol)	H_{peak} TDS (kJ/mol)
Soret	8.8 ± 0.2	9.7 ± 0.2	
A_0	8.7 ± 0.1	8.2 ± 0.4	8.2
A_1	9.1 ± 0.2	10.1 ± 0.5	10.0
A_3	10.4 ± 0.2	19.5 ± 0.6	18.3

The rebinding parameters were determined by flash photolysis in the Soret (Steinbach et al., 1991) and in the CO stretch bands (this work). Also listed is H_{peak} of the A substates obtained by temperature-derivative spectroscopy (TDS) (Berendzen and Braunstein, 1990). The Soret, A_0, and A_1 kinetics were fitted to a gamma distribution (Young and Bowne, 1984), and the A_3 and TDS kinetics to a Gaussian distribution.

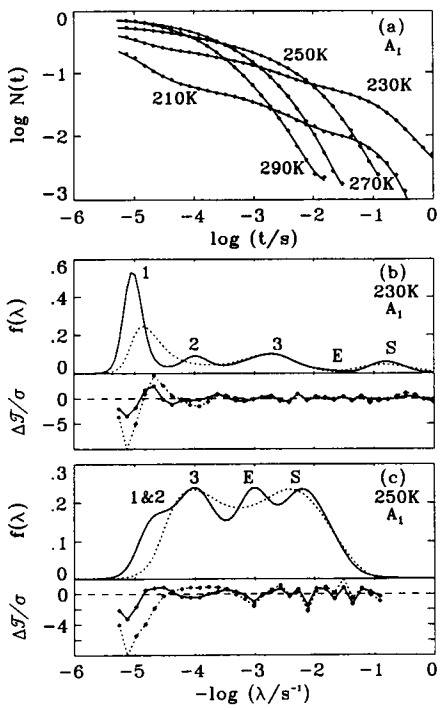

FIGURE 3 Rebinding kinetics and rate distributions of sperm whale MbCO measured in the A_1 band at $\nu \approx 1947$ cm^{-1}. Solvent: 75% glycerol/water (v/v), pH 5.7. (*a*) Fraction of unbound Mb, $N_1(t)$, between 200 and 300 K. Points represent the experimental data; curves give the kinetics calculated with Eq. 2 from the rate distributions $f_1(\lambda)$ obtained by the MEM. Distributions of rebinding rates $f_1(\lambda)$ at (*b*) 230 K and (*c*) 250 K. Also shown are the differences between the experimental transmittance and the transmittance calculated from $f_1(\lambda)$ with Eq. 2, $\Delta\mathcal{T}$, normalized to the statistical error, σ. For the traces shown, σ is $\sim 10^{-4}$ at all times. To illustrate the ability of MEM to extract the various peaks 1–3, E, and S, which are discussed in the text, the dashed curves show MEM calculations that were aborted before convergence of the algorithm ($\chi^2 = 5$), whereas the solid curves represent the final result ($\chi^2 = 1$).

$\chi^2 = 5$. The normalized residuals, $\Delta\mathcal{T}/\sigma$, show large systematic deviations, indicating that the fewer features in those rate distributions are inconsistent with the data. After convergence of the MEM algorithm to $\chi^2 = 1$, all peaks are present and the residuals are much smaller. We emphasize that the low noise, which is a direct consequence of logarithmic data averaging, is essential to resolution of the various peaks in rate distributions.

Peaks 1–3 are independent of the concentration of the CO in the solvent and therefore represent geminate processes. The position of peak S varies with the CO concentration in the solvent and represents the bimolecular binding of Mb and CO. Whereas the solvent process is nearly exponential in the dilute Soret samples (Fig. 2) because of pseudo-first-order conditions, the bimolecular conditions in the concentrated IR samples (Fig. 3) give rise to a nonexponential solvent rebinding. As explained below, peak E represents not a rebinding process but an interconversion among the *A* substates. Processes 1–3 occur before peak E; they represent rebinding on time scales faster than the *A* substate interconversion. Thus, they correspond to processes that occur within the individual substate populations. We discussed them in a previous paper (Nienhaus et al., 1994). Rebinding from the solvent, peak S, is slow compared with the interconversion and hence is governed by an average rate coefficient (Eq. 1).

Monitoring in the A_1 and A_3 bands

Fig. 4 shows IR data for CO rebinding with monitoring at the positions of the A_1 and A_3 bands at pH 9.1 in 75% glycerol/buffer at 220 and 250 K. For comparison we scaled the A_3 data to the A_1 data, using the population ratio determined at lower temperatures. At 220 K the A_3 trace is markedly above that of A_1 for times shorter than 10^4 s, indicating that less rebinding has occurred in A_3 up to that time. This result is consistent with the much higher barriers for the transition $B_3 \rightarrow A_3$, as measured below 160 K (Fig. 1). At $\approx 10^{-4}$ s the A_1 and A_3 traces merge, which we explain by the onset of fluctuations that lead to kinetic averaging. Thus, A_1 and A_3 are a single kinetic species at longer times, and the scaled kinetics measured in the individual *A* substates are identical (Steinbach et al., 1992). The geminate peak 3 and the bimolecular peak S are governed by averaged kinetics. With increasing temperature the point where the A_1 and A_3 kinetics meet moves to shorter times, and at 250 K the kinetics of the two substates become

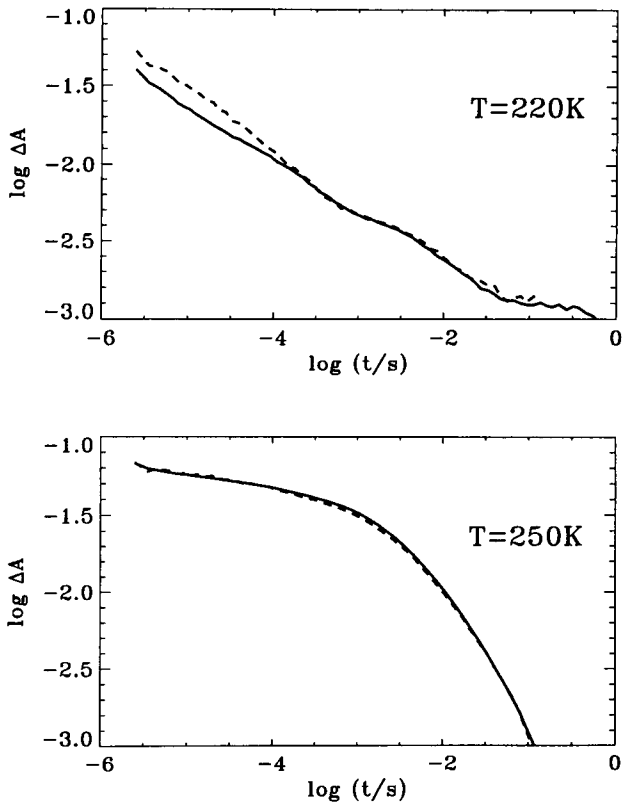

FIGURE 4 Rebinding kinetics of A_1 (*solid curves*) and A_3 (*dashed curves*) substates of MbCO at 220 and 250 K. The A_3 data were scaled to the A_1 data. Solvent: 75% glycerol/water (v/v), pH 9.1.

identical in the entire time range covered by the experiment (Fig. 4).

Monitoring in the A_0 band

The rebinding of photodissociated CO as measured in the A_0 band shown in Fig. 5 displays a surprising behavior: We would normally expect $N_0(t)$ to reflect only rebinding and thus to decrease monotonically with time. The actual behavior is different. At 230 K, for instance, $N_0(t)$ decreases until ~1 ms and then increases again. Because $N_0(t)$ gives the fraction of unbound Mb molecules in the A_0 substate, this behavior indicates that fewer CO molecules are bound in the substate A_0 at 10 than at 1 ms. Thermal dissociation is negligible at these temperatures; consequently, another explanation is needed.

Interconversion among the A substates explains the nonmonotonic behavior. Before the photolyzing flash the A bands represent the equilibrium population of the A substates. Immediately after photolysis the A bands have disappeared. With time, they reappear as the CO rebinds. Because A_0 rebinds faster than A_1, its population initially rises faster than that of A_1 and A_3, leading to population ratios A_0/A_1 and A_0/A_3 that are larger than in equilibrium. This situation prevails for times shorter than the inverse rate of transitions between A_0 and the other two substates. When the time approaches the inverse interconversion rate, a net population transfer from A_0 to A_1 and A_3 occurs until equilibrium is established. The data in Fig. 4 show that the rate coefficients for transitions between A_1 and A_3 are ~3 decades faster than the observed transfer of population out of A_0; A_1 and A_3 are thus in equilibrium and appear in the exchange with A_0 kinetically as one species, $A_1 + A_3$. At times longer than the interconversion between A_0 and $A_1 + A_3$, all three A substates maintain their equilibrium ratios until the ligands have completely rebound.

The fraction of the population transferred out of A_0 must appear in the rate distributions $f_1(\lambda)$ of A_1 and $f_3(\lambda)$ of A_3. Furthermore, the interconversion should not show up in the sum of the rate distributions of the three A bands or in the rate distribution from the Soret band. Comparison of Figs. 2 c and 4 c confirms that peak E shows up in the A_1 kinetics but not in the Soret kinetics.

The rate distribution $f_e(\lambda)$, attributed to the interconversion $A_0 \leftrightarrow A_1 + A_3$, has been extracted from the data by the global MEM and is shown in Fig. 6 for 230–300 K. As this method uses kinetic data from all three A substates, it provides the most precise measure of the position of peak 3. The temperature dependence of peak E yields information about the exchange mechanism. Peak E initially grows in area with increasing temperature, indicating an increase in the amount by which A_0 is out of equilibrium with $A_1 + A_3$ at the time the interconversion between them begins. Above 270 K the area of peak E decreases again, because most ligands escape into the solvent. Rebinding from the solvent is slower than the A state exchange and thus cannot produce the nonequilibrium situation that is needed for observation of peak E.

Gaussian fits to the exchange distribution $f_e(\lambda)$ at each temperature yielded the average rate coefficients for peak E, which were then fitted by an Arrhenius relation, $k(T) = A \exp(-E/RT)$, with a temperature-independent preexponential. The results of the fits are summarized in Table 2. The Arrhenius fits yield unphysically large preexponential factors. Such large values imply fluctuation phenomena in a complex, cooperative system and indicate that the Arrhenius relation is inappropriate (Bässler, 1987; Frauenfelder et al., 1991; Stillinger, 1995). Consequently, we use the Ferry relation (Ferry et al., 1953; Iben et al., 1989):

$$\kappa(T) = A_F \exp(-(E_F/RT)^2], \quad (4)$$

and plot the logarithm of the rate coefficients versus $(1000/T)^2$ in Fig. 7. The fit parameters are included in Table 2.

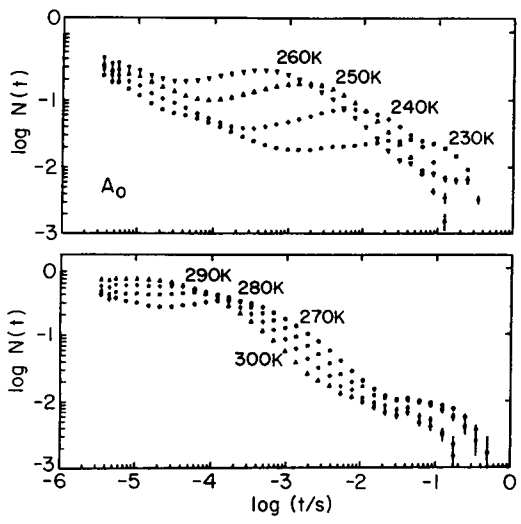

FIGURE 5 Kinetics of sperm whale MbCO (pH 5.7) measured in the A_0 band at $\nu \approx 1966\ cm^{-1}$. It represents the fraction of MbCO "missing" from the A_0 substate owing to both rebinding and interconversion to other A substates: (a) for 230–260 K, (b) for 270–300 K.

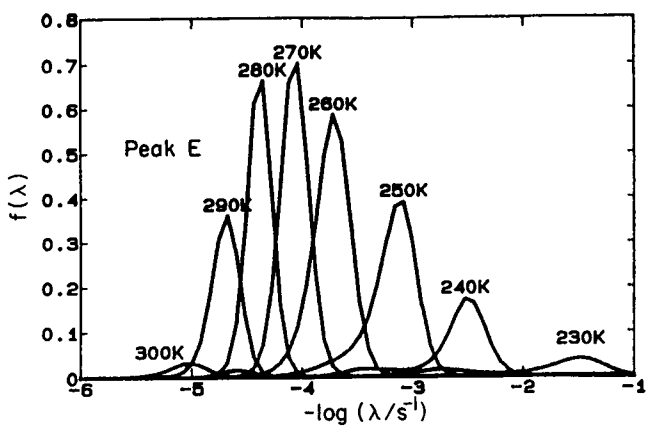

FIGURE 6 Temperature dependence of peak E between 230 and 300 K, determined by the global MEM. Peak E characterizes the interconversion $A_0 \leftrightarrow A_1 + A_3$.

TABLE 2 Temperature dependence of the interconversions $A_0 \leftrightarrow A_1 + A_3$ and $A_1 \leftrightarrow A_3$

Process	T Range (K)	$\log(A/s^{-1})$	E (kJ/mol)	$\log(A_F/s^{-1})$	E_F (kJ/mol)
$A_0 \leftrightarrow A_1 + A_3$	180–280	23 ± 4	95 ± 10	11.8 ± 1.4	9.3 ± 0.4
$A_1 \leftrightarrow A_3$	180–250	31 ± 4	120 ± 10	16.4 ± 1.4	9.9 ± 0.4

The data in Fig. 7 were fitted to an Arrhenius relation, $\kappa = A \exp(-E/RT)$, and a Ferry relation, Eq. 4.

DISCUSSION AND CONCLUSIONS

Relevance of low-temperature infrared kinetics

Traditionally, ligand binding data on heme proteins were collected with monitoring in the Soret band and analyzed by a least-squares fit, assuming a single functional form for $g(H_{BA})$ and a unique preexponential A_{BA}. However, the Soret band involves a superposition of bands for the different A substates with varying weights, depending on experimental conditions (Ansari et al., 1987; Mourant et al., 1993). The fact that the preexponential for rebinding to A_3 differs markedly from that of the other A states (Table 1) implies that the parameters obtained from the Soret data can only approximately model the kinetics (Steinbach et al., 1992).

We pointed out in the second subsection of Protein Substates and Function that the overall association rates for CO and O_2 binding increase when the pH is lowered. The pH dependence is consistent with a model that connects the association rates with the population in the A substates (Frauenfelder et al., 1989; Tian et al., 1993). Fig. 1 *d* shows that the A_0 substate, which becomes the dominant species at low pH, has smaller geminate barriers and thus rebinds faster than A_1 or A_3. The smaller geminate barrier leads to an increased overall binding rate coefficient (Steinbach et al., 1991). The connection between the distal pocket structure and the changes in the barrier at the heme iron in the different A substates needs further attention.

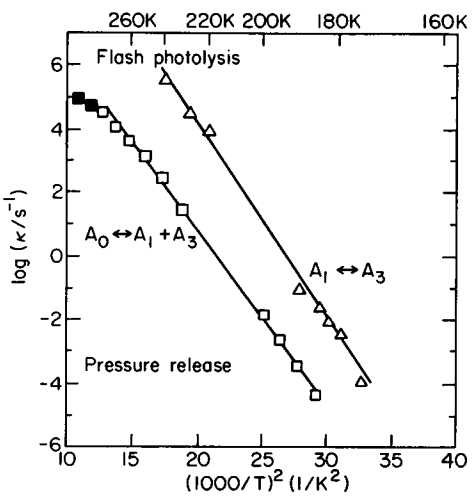

FIGURE 7 Characteristic rate coefficients for the interconversions $A_0 \leftrightarrow A_1 + A_3$ (□, ■) and $A_1 \leftrightarrow A_3$ (△) from IR flash photolysis and pressure relaxation experiments. Solid lines are fits of Eq. 4 to the data. ■, Rate coefficients excluded from the fits.

Interconversion between A_1 and A_3

Here we have studied the interconversion process $A_1 \leftrightarrow A_3$ above 200 K, using flash photolysis with IR monitoring. Previously we had investigated this process below 200 K on longer time scales with a pressure jump perturbation and Fourier-transform IR monitoring (Iben et al., 1989; Scholl, 1991). The pressure jump studies showed that the interconversion $A_1 \leftrightarrow A_3$ is $\sim 10^3$ times faster than the interconversion $A_0 \leftrightarrow A_1 + A_3$, demonstrating that A_1 and A_3 are in equilibrium before interconversion from A_0 starts. This result is confirmed by the data in Fig. 4, which allow us to estimate the interconversion rate coefficients $\kappa_3 = \kappa_{13} + \kappa_{31}$. Here, κ_{13} and κ_{31} denote the rate coefficients for the transitions $A_1 \rightarrow A_3$ and $A_1 \leftarrow A_3$. These data are shown in Fig. 7 together with the rate coefficients from the pressure studies (Iben et al., 1989; Scholl, 1991). The curves are fits to both flash photolysis and pressure data using the Ferry relation, Eq. 4, with parameters A_F and E_F listed in Table 2.

Interconversion between A_0 and $A_1 + A_3$

The present study of the interconversion process $A_0 \leftrightarrow A_1 + A_3$ with flash photolysis in the IR extends our previous study with a pressure relaxation technique (Iben et al., 1989; Frauenfelder et al., 1990). Because of its limited time resolution ($t > 10$ s), the pressure relaxation was able to measure the interconversion only below 200 K, whereas the IR flash photolysis yields data between 200 and 300 K with microsecond time resolution. The IR kinetics and the pressure relaxation experiments measure the rate coefficient $\kappa_0 = \kappa_{01} + \kappa_{10}$, where κ_{01} and κ_{10} denote the rate coefficients for the transitions $A_0 \rightarrow A_1 + A_3$ and $A_0 \leftarrow A_1 + A_3$. With κ_0 and the equilibrium ratio $A_0/(A_1 + A_3)$ the individual rate coefficients can be determined.

Fig. 7 shows the average rate coefficients for this interconversion as obtained from the two methods, plotted as a function of $(1000/T)^2$. Pressure relaxation actually shows a fast exponential and a slow nonexponential component (Frauenfelder et al., 1990). Inasmuch as the fast component accounts for ≈90% of the magnitude of the interconversion, we use the rate coefficient of this component for the comparison with κ_0 from the IR kinetics data. The IR kinetics do not reveal the details of the interconversion kinetics and are, therefore, analyzed only in terms of an average rate coefficient $\langle\kappa_0\rangle$. Fig. 7 shows saturation behavior at higher temperatures, which we discuss below. Up to 280 K, however, the average rate coefficients $\langle\kappa_0\rangle$ from both techniques can be fitted well with a single straight line plotted as a function

of $(1000/T)^2$. The Ferry law, Eq. 4, consequently describes the interconversion $A_0 \leftrightarrow A_1 + A_3$ over 8 decades in time. The parameters A_F and E_F resulting from a fit to the entire temperature range are listed in Table 2. The fact that the two data sets match well implies that the rate with which A_0 and $A_1 + A_3$ return to equilibrium is insensitive to the perturbation that creates the nonequilibrium situation. An Arrhenius fit to the data in Fig. 7 over the same temperature range deviates significantly from the experimental data. This Ferry behavior implies dynamics on a rough potential energy surface and demonstrates a similarity between proteins and glasses (Iben et al., 1989; Frauenfelder et al., 1990).

Connections among structure, kinetics, and function

In recent years substantial progress has been made in understanding the structural features that give rise to the different A substate bands. Earlier x-ray (Kuriyan et al., 1986) and neutron (Cheng and Schoenborn, 1991) structures had been refined with multiple positions of the bound CO, suggesting different geometries of the heme-CO unit in the different A substates. These structures showed large bending angles α of the CO with respect to the heme normal in the range 40°–60°. However, a linear Fe-C-O geometry is electronically favorable and normally seen in small heme model compounds (Li and Spiro, 1988). The large distortion in MbCO was thought to arise from a repulsion between the CO and the His-E7 imidazole sidechain. Molecular dynamics simulations (Case and Karplus, 1978; Kuczera et al., 1990; Jewsbury and Kitagawa, 1994) and Debye–Waller factors (Kuriyan et al., 1986) indicate that the His-E7 sidechain is relatively mobile, and it is hard to rationalize that that sidechain can exert enough force to bend the CO away from the favored perpendicular geometry. Linear dichroism measurements gave independent information about the geometry of the Fe-C-O unit and revealed much smaller angles (Moore et al., 1988; Ormos et al., 1988). The most recent studies reported $\alpha < 10°$ (Ivanov et al., 1994; Lim et al., 1995). The discrepancy between the crystallographic and spectroscopic observations still awaits a satisfactory explanation.

Although vibrational spectroscopy cannot give direct structural information, it is an exceedingly sensitive gauge of interactions between ligand and protein. Therefore, once the interactions are understood, very precise structural information can be obtained. Both ν_{FeC} and ν_{CO} have been studied extensively. To explain the different A substate frequencies, a variety of models have been proposed that are based on the influence of electrostatic fields on the extent of backbonding from the heme iron to the CO ligand. This explanation implies an inverse correlation between ν_{FeC} and ν_{CO}, as has been observed experimentally (Tsubaki et al., 1985; Paul et al., 1985; Li and Spiro, 1988; Park et al., 1991; Ray et al., 1994). Recent Fourier-transform IR studies on many distal pocket mutants support this model and give some insight into the nature of the A substates (Balasubramanian et al., 1993; Braunstein et al., 1993; Li et al., 1994). Mutants in which His-E7 is replaced by an amino acid with a small, aliphatic sidechain show only one A substate at the position of A_0 (Braunstein et al., 1993; Li et al., 1994). This result implies that the His-E7 sidechain in native MbCO does not interact with the bound CO in the A_0 substate. The A_0 population is pH dependent in native MbCO, consistent with a protonation of the imidazole sidechain of His-E7. This transition has a very low pK_a for a histidine of ≈4.5, reflecting its low-polarity heme pocket environment (Wilbur and Allerhand, 1977; Fuchsman and Appleby, 1979; Ramsden and Spiro, 1989). On protonation, the sidechain is expected to extend out of the hydrophobic heme pocket into the polar solvent. Indeed, the x-ray structure of MbCO at pH 4, where A_0 is enhanced, shows that the His-E7 sidechain has swung out of the distal pocket (Quillin et al., 1992; Yang and Phillips, 1995). Therefore, this open distal pocket structure has been associated with the A_0 substate (Zhu et al., 1992, Braunstein et al., 1993; Jewsbury and Kitagawa, 1994; Ray et al., 1994; Li et al., 1994).

Both A_1 and A_3 are present at higher pH. The imidazole sidechain is uncharged for these two substates and resides inside the heme pocket, as seen in the x-ray (Kuriyan et al., 1986; Quillin et al., 1993), neutron (Cheng and Schoenborn, 1991), and NMR (Ösapay et al., 1994) structures. In all these structures A_1 and A_3 cannot be distinguished, and the assignment of the structural differences on the basis of spectroscopic data is still ambiguous. Oldfield et al. (1991) proposed a model that explained the A substate lines by electrostatic interactions between the CO dipole and four different orientations of the dipole associated with the imidazole sidechain, arising from two ring-flip isomers of the His-E7 sidechain in combination with two tautomers ($H^{\delta 1}$/$H^{\epsilon 2}$). Spiro and collaborators (Ray et al., 1994) assigned A_1 and A_3 to two different tautomers of the distal imidazole, with the proton on N_ϵ and N_δ, respectively. In A_1 the positive charge on the N_ϵ proton is responsible for the lower frequency of 1945 cm^{-1}, compared with 1966 cm^{-1} in the absence of polar interactions. For A_3 they assumed a lone pair interaction of N_ϵ with the CO π^* orbital, as originally proposed by Maxwell and Caughey (1976). Because A_1 is the dominant substate in solution at pH 5.7, one should expect a protonated N_ϵ in the neutron structure of MbCO ($P2_1$ crystals), but the proton is not present (Cheng and Schoenborn, 1991). To reconcile their assignment with the neutron data, Ray et al. (1994) argue that A_3 may be the dominant substate in the monoclinic crystal. Indeed, in crystals, a larger fraction of A_3 can be observed under certain not well-understood conditions (Makinen et al., 1979; Mourant et al., 1993). We have seen A_3 populations as large as 90% in orthorhombic crystals that were partially met-Mb (Mourant et al., 1993). Our preparations with monoclinic crystals, however, never showed a dominant A_3 component. The model of Ray et al. (1994) was recently criticized by Jewsbury and Kitagawa (1994) on the basis of their MD simulations. In these calculations the His-E7 im-

idazole positioned itself such that the protonated nitrogen pointed into the heme pocket, in disagreement with the neutron structure. Protonation of N_ϵ led to a long-lived interaction with the CO. This configuration was identified with A_3. The N_δ tautomer interacted more weakly with the CO, and hence it was assigned to A_1.

Our measurements of the interconversion rate coefficients give additional insights into the nature of the A substates. The $A_0 \leftrightarrow A_1 + A_3$ interconversion is cooperative and characterized by a steep temperature dependence, as seen in Fig. 7. What molecular mechanism is responsible for this transition? The His-E7 imidazole is buried inside the heme pocket in the A_1 and A_3 substates. Transition to the A_0 substate involves protonation of the His-E7 imidazole sidechain. The chemical nature and the kinetics of protonation–deprotonation processes of buried residues has been elucidated by hydrogen-exchange experiments in great detail. The chemical exchange of a labile proton in the protein interior happens by either "local unfolding" or "solvent penetration" (Woodward et al., 1982; Englander and Kallenbach, 1984). Measurements of the hydrogen exchange of the His-E7 N_ϵ proton in the high-pH (closed) form of MbCN with NMR have been explained by a mechanism involving a transient conformational change to an open state that exposes the imidazole to the solvent (Lecomte and La Mar, 1985; Lambright et al., 1989) in which the exchange of imidazole NH protons is catalyzed by OH^- or H^+ (Woodward et al., 1982; Lecomte and La Mar, 1985). The contribution from water to the proton exchange is usually negligible (Lambright et al., 1989). According to the low-pH crystal structure, exposure of the imidazole side to the solvent involves rotation of the distal histidine around the $C_{[\alpha]}$—$C_{[\beta]}$ bond. To accommodate that motion, reorientation of Arg CD3, Asp-E3, the E helix, and the CD corner as well as solvent molecules is necessary.

The steep temperature dependence of protein conformational changes implies that protonation–deprotonation could become rate limiting at higher temperatures. With the bimolecular protonation rate coefficient of imidazole in aqueous solution at 298 K, $1.5 \times 10^{10}\ M^{-1}\ s^{-1}$ (Eigen, 1964), and a pK of $\approx$4.5 of the His-E7 sidechain, we estimate a deprotonation rate coefficient of $\sim 5 \times 10^5\ s^{-1}$ in the transition $A_0 \rightarrow A_1$. The flattening of the temperature dependence of κ_0 observed above 270 K (Fig. 7) could, therefore, reflect rate limitation that is due to protonation–deprotonation. There is, however, another reason for this behavior. Because the A substate transitions are cooperative motions, they are strongly coupled to the solvent dynamics. The relaxation rate of glycerol starts deviating markedly from the Ferry relation above 270 K toward lower rates (Bässler, 1987). Consequently, the A substate interconversion rate κ_0 follows this trend.

The interconversion rate coefficient of $A_1 \leftrightarrow A_3$ is more than 3 orders of magnitude faster than the $A_0 \leftrightarrow A_1 + A_3$ exchange (Fig. 7); extrapolation of the $A_1 \leftrightarrow A_3$ rate to room temperature yields $\sim$1 ns. The much faster interconversion suggests less structural reorientation than in the $A_0 \leftrightarrow A_1 + A_3$ process. In the model of Jewsbury and Kitagawa (1994) the $A_1 \leftrightarrow A_3$ exchange involves an imidazole ring rotation and a protonation change. From NMR studies it is well known that internal sidechains rotate very slowly. For example, ring flips of buried phenylalanine sidechains in BPTI have been observed on the millisecond time scale at 300 K (Wagner and Wüthrich, 1986). A faster isomerization could occur by transient rotation of the imidazole out of the heme pocket. Such a motion should result in a rate similar to that of $A_0 \leftrightarrow A_1 + A_3$. Although the model of Spiro and collaborators (Ray et al., 1994) avoids isomerization, it also involves a change in protonation between $N\epsilon$ and N_δ in the $A_1 \leftrightarrow A_3$ exchange.

If a large conformational change is indeed necessary to change the protonation of His-E7, the fast $A_1 \leftrightarrow A_3$ interconversion cannot be associated with a protonation change. Consequently, the most likely model for the two substates has the proton attached to $N\epsilon$ in both A_1 and A_3. Subtle interactions between His-E7 and its environment lead to one substate, A_1, with less and one substate, A_3, with more interaction between the proton and the CO. Different amounts of downshift of the IR lines from the A_0 frequency arise from the different interactions. Such a model makes sense in light of the following observations: The fraction of A_3 is significantly larger in some proximal mutants of myoglobin (Abadan et al., 1995). It is difficult to see why proximal modifications should affect the equilibrium between tautomer–isomer states of the distal imidazole. However, proximal changes can lead to a slightly altered conformation of the heme in the apoprotein, which can modify the steric relation between the CO and the His-E7. Li et al. (1994) have shown that a number of mutants at position B10, which is in contact with the imidazole sidechain, have a substantially increased A_3 fraction, with the leucine-to-phenylalanine replacement showing only a single IR band at 1933 cm^{-1}, the position of A_3. Most likely, changes at position B10 lead to a slightly modified structure of His-E7, so an A_3-type interaction between the imidazole and the CO becomes more favorable.

In recent years several groups of researchers have investigated conformational changes in myoglobin after ligand dissociation that reveal themselves in the shift of spectral bands (band III, Soret) and in the changes of the rebinding barriers at the heme iron (Steinbach et al., 1991; Nienhaus et al., 1992, 1994; Tian et al., 1992; Lambright et al., 1993, Jackson et al., 1994; Ansari et al., 1994; Panchenko et al., 1995). These phenomena are associated with relaxations involving the proximal side of the heme. Jackson et al. (1994) modeled their band III relaxation data with a stretched exponential and obtained parameters in agreement with extrapolations of the low-temperature data by Steinbach et al. (1991). At 300 K (in glycerol–buffer solvent), $\sim$90% of the shift of band III occurs on time scales shorter than a nanosecond. By contrast, the interconversion time for $A_0 \leftrightarrow A_1 + A_3$ is 10 μs, and extrapolation yields $\sim$1 ns for $A_1 \leftrightarrow A_3$. Both A substate interconversion and proximal relaxation are sensitive to solvent viscosity, indicating that

they are not local but global motions (Young et al., 1991; Ansari et al., 1994). The proximal relaxation, however, is much faster. The different time dependencies reflect the widely different free energy barriers between conformational substates in the various tiers of the substate hierarchy (Frauenfelder et al., 1991).

This research was supported by grants from the National Science Foundation (DMB87-16476) and the National Institutes of Health (GM 18051). R.D.Y. thanks the Department of Physics and the Graduate School of Illinois State University for research support.

REFERENCES

Abadan, Y., E. Y. T. Chien, K. Chu, C. D. Eng, G. U. Nienhaus, and S. O. Sligar. 1995. Ligand binding to heme proteins. V. Light-induced relaxation in proximal mutants L89I and H97F of carbonmonoxymyoglobin. *Biophys. J.* 68:2497–2504.

Alben, J. O., D. Beece, S. F. Bowne, W. Doster, L. Eisenstein, H. Frauenfelder, D. Good, J. D. McDonald, M. C. Marden, P. P. Moh, L. Reinisch, A. H. Reynolds, E. Shyamsunder, and K. T. Yue. 1982. Infrared spectroscopy of photodissociated carboxymyoglobin at low temperatures. *Proc. Natl. Acad. Sci. USA.* 79:3744–3748.

Alben, J. O., P. P. Moh, F. G. Fiamingo, and R. A. Altschuld. 1981. Cytochrome oxidase (aa_3) heme and copper observed by low temperature Fourier transform infrared spectroscopy of the CO complex. *Proc. Natl. Acad. Sci. USA.* 78:234–237.

Ansari, A., J. Berendzen, S. F. Bowne, H. Frauenfelder, I. E. T. Iben, T. B. Sauke, E. Shyamsunder, and R D. Young. 1985. Protein states and proteinquakes. *Proc. Natl. Acad. Sci. USA.* 82:5000–5004.

Ansari, A., J. Berendzen, D. Braunstein, B. R. Cowen, H. Frauenfelder, M. K. Hong, I. E. T. Iben, J. B. Johnson, P. Ormos, T. B. Sauke, R. Scholl, A. Schulte, P. J. Steinbach, J. Vittitow, and R. D. Young. 1987. Rebinding and relaxation in the myoglobin pocket. *Biophys. Chem.* 26: 337–355.

Ansari, A., C. M. Jones, E. R. Henry, J. Hofrichter, and W. A. Eaton. 1994. Conformational relaxation and ligand binding in myoglobin. *Biochemistry.* 33:5128–5145.

Austin, R. H., K. W. Beeson, L. Eisenstein, H. Frauenfelder, and I. C. Gunsalus. 1975. Dynamics of ligand binding to myoglobin. *Biochemistry.* 14:5355–5373.

Balasubramanian, S., D. G. Lambright, M. C. Marden, and S. G. Boxer. 1993. CO recombination to human myoglobin mutants in glycerol-water solutions. *Biochemistry.* 32:2202–2212.

Bässler, H. 1987. Viscous flow in supercooled liquids analyzed in terms of transport theory for random media with energetic disorder. *Phys. Rev. Lett.* 58:767–770.

Berendzen, J. 1990. Rate-window methods and myoglobin dynamics. Ph.D. dissertation. University of Illinois at Urbana-Champaign.

Berendzen, J., and D. Braunstein. 1990. Temperature-derivative spectroscopy: a tool for protein dynamics. *Proc. Natl. Acad. Sci. USA.* 87:1–5.

Braunstein, D. P., K. Chu, K. D. Egeberg, H. Frauenfelder, J. R. Mourant, G. U. Nienhaus, P. Ormos, S. G. Sligar, B. A. Springer, and R. D. Young, 1993. Ligand binding to heme proteins. III. FTIR studies of His-E7 and Val-E11 mutants of carbonmonoxymyoglobin. *Biophys. J.* 65:2447–2454.

Case, D. A., and M. Karplus. 1978. Stereochemistry of carbon monoxide binding to myoglobin and hemoglobin. *J. Mol. Biol.* 123:697–701.

Cheng, X., and B. P. Schoenborn. 1991. Neutron diffraction study of carbonmonoxy myoglobin. *J. Mol. Biol.* 220:381–399.

Doster, W., D. Beece, S. F. Bowne, E. E. DiIorio, L. Eisenstein, H. Frauenfelder, L. Reinisch, E. Shyamsunder, K. H. Winterhalter, and K. T. Yue. 1982. Control and pH dependence of ligand binding to heme proteins. *Biochemistry.* 21:4831–4839.

Doster, W., S. F. Bowne, H. Frauenfelder, L. Reinisch, and E. Shyamsunder. 1987. Recombination of carbon monoxide to ferrous horseradish peroxidase types A and C. *J. Mol. Biol.* 194:299–312.

Ehrenstein, D., M. Filiaci, B. Scharf, M. Engelhard, P. J. Steinbach, and G. U. Nienhaus. 1995. Ligand binding and protein dynamics in cupredoxins. *Biochemistry.* 34:12170–12177.

Eigen, M. 1964. Proton transfer, acid-base catalysis, and enzymatic hydrolysis. *Angew. Chemie Int. Ed. Eng.* 3:1–19.

Elber, R., and M. Karplus. 1987. Multiple conformational states of proteins: a molecular dynamics analysis of myoglobin. *Science.* 235: 318–321.

Englander, S. W., and N. R. Kallenbach. 1984. Hydrogen exchange and structural dynamics of proteins and nucleic acids. *Q. Rev. Biophys.* 16:521–655.

Ferry, J. D., L. D. Grandine, Jr., and E. R. Fitzgerald. 1953. The relaxation distribution function of polyisobutylene in the transition from rubber-like to glass-like behavior. *J. Appl. Phys.* 24:911–916.

Frauenfelder, H., N. A. Alberding, A. Ansari, D. Braunstein, B. R. Cowen, M. K. Hong, I. E. T. Iben, J. B. Johnson, S. Luck, M. C. Marden, J. R. Mourant, P. Ormos, L. Reinisch, R. Scholl, A. Schulte, E. Shyamsunder, L. B. Sorenson, P. J. Steinbach, A. Xie, R. D. Young, and K. T. Yue. 1990. Proteins and pressure. *J. Phys. Chem.* 94:1024–1038.

Frauenfelder, H., F. Parak, and R. D. Young. 1988. Conformational substates in proteins. *Annu. Rev. Biophys. Biophys. Chem* 17:451–479.

Frauenfelder, H., G. A. Petsko, and D. Tsernoglou. 1979. Temperature-dependent x-ray diffraction as a probe of protein structural dynamics. *Nature (Lond.).* 280:558–563.

Frauenfelder, H., S. G. Sligar, and P. G. Wolynes. 1991. The energy landscapes and motions of proteins. *Science.* 254:1598–1603.

Frauenfelder, H., P. J. Steinbach, and R. D. Young. 1989. Conformational relaxation in proteins. *Chem. Scr.* 29A:145–150.

Fuchsman, W. H., and C. A. Appleby. 1979. CO and O_2 complexes of soybean leghemoglobins: pH effects upon infrared and visible spectra. Comparisons with CO and O_2 complexes of myoglobin and hemoglobin. *Biochemistry.* 18:1309–1321.

Henry, E. R. 1993. Molecular dynamics simulations of heme reorientational motions in myoglobin. *Biophys. J.* 64:869–885.

Hong, M. K., D. Braunstein, B. R. Cowen, H. Frauenfelder, I. E. T. Iben, J. R. Mourant, P. Ormos, R. Scholl, A. Schulte, P. J. Steinbach, A. H. Xie, and R. D. Young. 1990. Conformational substates and motions in myoglobin: external influences on structure and dynamics. *Biophys. J.* 58:429–436.

Honeycutt, J. D., and D. Thirumalai. 1990. Metastability of the folded states of globular proteins. *Proc. Natl. Acad. Sci. USA.* 87:3526–3529.

Hvidt, A., and S. Nielsen. 1966. Hydrogen exchange in proteins. *Adv. Protein Chem.* 21:287–386.

Iben, I. E. T., D. Braunstein, W. Doster, H. Frauenfelder, M. K. Hong, J. B. Johnson, S. Luck, P. Ormos, A. Schulte, P. J. Steinbach, A. H. Xie, and R. D. Young. 1989. Glassy behavior of a protein. *Phys. Rev. Lett.* 62:1916–1919.

Ivanov, D., J. T. Sage, M. Keim, J. R. Powell, S. A. Asher, and P. M. Champion. 1994. Determination of CO orientation in myoglobin by single-crystal infrared linear dichroism. *J. Am. Chem. Soc.* 116: 4139–4140.

Jackson, T. A., M. Lim, and P. A. Anfinrud. 1994. Complex nonexponential relaxation in myoglobin after photodissociation of MbCO: measurement and analysis from 2 ps to 56 μs. *Chem. Phys.* 180:131–140.

Jewsbury, P., and T. Kitagawa. 1994. The distal residue-CO interaction in carbonmonoxy myoglobins: a molecular dynamics study of the two distal histidine tautomers. *Biophys. J.* 67:2236–2250.

Jung, C., G. Hui Bon Hoa, K.-L. Schröder, M. Simon, and J. P. Doucet. 1992. Substrate analogue induced changes of the CO-stretching mode in the cytochrome P450cam-carbon monoxide complex. *Biochemistry.* 31: 12,855–12,862.

Kuczera, K., J. Kuriyan, and M. Karplus. 1990. Temperature dependence of the structure and dynamics of myoglobin. *J. Mol. Biol.* 213:351–373.

Kuriyan, J., S. Wilz, M. Karplus, and G. A. Petsko. 1986. X-ray structure and refinement of carbon-monoxy (Fe II)-myoglobin at 1.5 angstrom resolution. *J. Mol. Biol.* 192:133–154.

Lambright, D. G., S. Balasubramanian, and S. G. Boxer. 1989. Ligand and proton exchange dynamics in recombinant human myoglobin mutants. *J. Mol. Biol.* 207:289–299.

Lambright, D. G., S. Balasubramanian, and S. G. Boxer. 1993. Dynamics of protein relaxation in site-specific mutants of human myoglobin. *Biochemistry.* 32:10116–10124.

Lecomte, J. T. J., and G. N. La Mar. 1985. ^{1}H NMR studies of labile proton exchange in the heme cavity as a probe for the potential ligand entry channel in myoglobin. *Biochemistry.* 24:7388–7395.

Li, T., M. L. Quillin, G. N. Phillips, Jr., and J. S. Olson. 1994. Structural determinants of the stretching frequency of CO bound to myoglobin. *Biochemistry.* 33:1433–1446.

Li, X. Y., and T. G. Spiro. 1988. Is bound CO linear or bent in heme proteins? Evidence from resonance Raman and infrared spectroscopic data. *J. Am. Chem. Soc.* 110:6024–6033.

Lim, M., T. A. Jackson, and P. A. Anfinrud. 1995. Binding of CO to myoglobin from a heme pocket docking site to form nearly linear Fe-C-O. *Science.* 269:962–966.

Makinen, M. W., R. A. Houtchens, and W. S. Caughey. 1979. Structure of carboxymyoglobin in crystals and in solution. *Proc. Natl. Acad. Sci. USA.* 76:6042–6046.

Maxwell, J. C., and W. S. Caughey. 1976. An infrared study of NO bonding to heme B and hemoglobin A. Evidence for inositol hexaphosphate induced cleavage of proximal histidine to iron bonds. *Biochemistry.* 15:388–395.

Moore, J. H., P. A. Hansen, and R. A. Hochstrasser. 1988. Iron-carbonyl bond geometries of carboxymyoglobin and carboxyhemoglobin in solution determined by picosecond time-resolved infrared spectroscopy. *Proc. Natl. Acad. Sci. USA.* 85:5062–5066.

Morikis, D., P. M. Champion, B. A. Springer, and S. G. Sligar. 1989. Resonance Raman investigations of site-directed mutants of myoglobin: effects of distal histidine replacement. *Biochemistry.* 28:4791–4800.

Mourant, J. R., D. Braunstein, K. Chu, H. Frauenfelder, G. U. Nienhaus, P. Ormos, and R. D. Young. 1993. Ligand binding to heme proteins. II. Transitions in the heme pocket of myoglobin. *Biophys. J.* 65: 1496–1507.

Nar, H., A. Messerschmidt, R. Huber, M. van de Kamp, and G. W. Canters. 1991. Crystal structure analysis of oxidized *Pseudomonas aeruginosa* azurin at pH 5.5 and pH 9.0, a pH-induced conformational transition involves a peptide bond flip. *J. Mol. Biol.* 221:765–772.

Nienhaus, G. U., J. R. Mourant, and H. Frauenfelder. 1992. Spectroscopic evidence for conformational relaxation in myoglobin. *Proc. Natl. Acad. Sci. USA.* 89:2902–2906.

Nienhaus, G. U., J. R. Mourant, K. Chu, and H. Frauenfelder. 1994. Ligand binding to heme proteins. The effect of light on ligand binding in myoglobin. *Biochemistry.* 33:13,413–13,430.

Oldfield, E., K. Guo, J. D. Augspurger, and C. E. Dykstra. 1991. A molecular model for the major conformational substates in heme proteins. *J. Am. Chem. Soc.* 113:7537–7541.

Ormos, P., D. Braunstein, H. Frauenfelder, M. K. Hong, S.-L. Lin, T. S. Sauke, and R. D. Young. 1988. Orientation of carbon monoxide and structure-function relationship in carbonmonoxymyoglobin. *Proc. Natl. Acad. Sci. USA.* 85:8492–8496. Ösapay, K., Y. Theriault, P. E. Wright, and D. A. Case. 1994. Solution structure of carbonmonoxy myoglobin determined from nuclear magnetic resonance distance and chemical shift constraints. *J. Mol. Biol.* 244:183–197.

Panchenko, A. R., J. Wang, G. U. Nienhaus, and P. G. Wolynes. 1995. Analysis of ligand binding to heme proteins using a fluctuating path description. *J. Phys. Chem.* 99:9278–9282.

Park, K. D., K. Guo, F. Adebodun, M. L. Chiu, S. G. Sligar, and E. Oldfield. 1991. Distal and proximal ligand interactions in heme proteins: correlations between C-O and Fe-C vibration frequencies, oxygen-17 and carbon-13 nuclear magnetic resonance chemical shifts, and oxygen-17 nuclear quadrupole coupling constants in C^{17}O- and ^{13}CO-labeled species. *Biochemistry.* 30:2333–2347.

Paul, J., M. L. Smith, and K. G. Paul. 1985. The vibrational bands of carbon monoxide bound to hemes or metal surfaces. *Biochim. Biophys. Acta.* 832:257–264.

Porter, T. D., and M. J. Coon. 1991. Cytochrome P450. *J. Biol. Chem.* 266:13,469–13,472.

Potter, W. T., J. H. Hazzard, M. G. Choc, M. P. Tucker, and W. S. Caughey. 1990. Infrared spectra of carbonyl hemoglobins: characterization of dynamic heme pocket conformers. *Biochemistry.* 29:6283–6295.

Quillin, M. L., R. M. Arduini, J. S. Olson, and G. N. Phillips, Jr. 1993. High resolution crystal structures of distal histidine mutants of sperm whale myoglobin. *J. Mol. Biol.* 234:140–155.

Quillin, M. L., R. E. Brantley, Jr., K. A. Johnson, and G. Phillips. 1992. Kinetic and structural analysis of the effects of pH on carbon monoxide association in myoglobin. *Biophys. J.* 61:A466.

Ramsden, J., and T. G. Spiro. 1989. Resonance Raman evidence that distal histidine protonation removes the steric hindrance to upright binding of carbon monoxide to myoglobin. *Biochemistry.* 28:3125–3128.

Ray, G. B., X.-Y. Li, J. A. Ibers, J. L. Sessler, and T. G. Spiro. 1994. How far can proteins bend the FeCO unit? Distal polar effects in heme proteins and models. *J. Am. Chem. Soc.* 116:162–176.

Scholl, R. 1991. Relaxation dynamics in heme proteins. Ph.D. dissertation. University of Illinois at Urbana-Champaign.

Shimada, H., and W. S. Caughey. 1982. Dynamic protein structures. *J. Biol. Chem.* 257:11893–11900.

Springer, B. A., S. G. Sligar, J. S. Olson, and G. N. Phillips, Jr. 1994. Mechanism of ligand recognition in myoglobin. *Chem. Rev.* 94: 699–714.

Steinbach, P. J., A. Ansari, J. Berendzen, D. Braunstein, K. Chu, B. Cowen, D. Ehrenstein, H. Frauenfelder, J. B. Johnson, D. C. Lamb, S. Luck, J. R. Mourant, G. U. Nienhaus, P. Ormos, R. Philipp, A. Xie, and R. D. Young. 1991. Ligand binding to heme proteins: the connection between dynamics and function. *Biochemistry.* 30:3988–4001.

Steinbach, P. J., K. Chu, H. Frauenfelder, J. B. Johnson, D. C. Lamb, G. U. Nienhaus, T. B. Sauke, and R. D. Young. 1992. Determination of rate distributions from kinetic experiments. *Biophys. J.* 61:235–245.

Stillinger, F. H. 1995. A topographic view of supercooled liquids and glass formation. *Science.* 267:1935–1939.

Tian, W. D., J. T. Sage, and P. M. Champion. 1993. Investigations of ligand association and dissociation rates in the "open" and "closed" states of myoglobin. *J. Mol. Biol.* 233:155–166.

Tian, W. D., J. T. Sage, V. Šrajer, and P. M. Champion. 1992. Relaxation dynamics of myoglobin in solution. *Phys. Rev. Lett.* 68:408–412.

Tsubaki, M., A. Hiwatashi, and Y. Ichikawa. 1986. Effects of cholesterol and adrenodoxin binding on the heme moiety of cytochrome P450$_{scc}$: a resonance Raman study. *Biochemistry.* 35:3563–3569.

Tsubaki, M., and Y. Ichikawa. 1985. Resonance Raman detection of a ν (Fe-CO) stretching frequency in cytochrome *P*-450$_{scc}$ from bovine adrenocortical mitochondria. *Biochim. Biophys. Acta.* 827:268–274.

Uno, T., Y. Nishimura, M. Tsuboi, R. Makino, T. Iizuka, and Y. Ichikawa. 1987. Two types of conformers with distinct Fe-C-O configuration in the ferrous CO complex of horseradish peroxidase. *J. Biol. Chem.* 262: 4549–4556.

Wagner, G., and K. Wüthrich. 1986. Observation of internal motility of proteins by nuclear magnetic resonance in solution. *In* Methods in Enzymology, Vol. 131. C. H. W. Hirs and S. N. Timasheff, editors. Academic Press, New York. 307–326.

Wilbur, D. J., and A. Allerhand. 1977. Titration behavior and tautomeric states of individual histidine residues of myoglobins. *J. Biol. Chem.* 252:4968–4975.

Woodward, C., I. Simon, and E. Tüchsen. 1982. Hydrogen exchange and the dynamic structure of proteins. *Mol. Cell. Biochem.* 48:135–160.

Yang, F., and G. N. Phillips, Jr. 1995. Structures of CO-, deoxy-, and met-myoglobin at various p*H* values. *J. Mol. Biol.* 256:762–774.

Young, R. D., and S. F. Bowne. 1984. Conformational substates and barrier height distributions in ligand binding to heme proteins. *J. Chem. Phys.* 81:3730–3737.

Young R. D., H. Frauenfelder, J. B. Johnson, D. C. Lamb, G. U. Nienhaus, R. Phillip, and R. Scholl. 1991. Time- and temperature dependence of large-scale conformational transitions in myoglobin. *Chem. Phys.* 158: 315–328.

Zhu, L., J. T. Sage, A. A. Rigos, D. Morikis, and P. M. Champion. 1992. Conformational interconversion in protein crystals. *J. Mol. Biol.* 224: 207–215.